



The 2016 record-breaking marine heatwave in the Yellow Sea and associated atmospheric circulation anomalies



Yan Li ^{a,b}, Guoyu Ren ^{b,c}, Qinglong You ^d, Qingyuan Wang ^e, Qianru Niu ^a, Lin Mu ^{a,*}

^a College of Life Sciences and Oceanography, Shenzhen University, Shenzhen, China

^b Department of Atmospheric Science, School of Environmental Studies, China University of Geosciences, Wuhan, China

^c Laboratory for Climate Studies, National Climate Center, China Meteorological Administration, Beijing, China

^d Department of Atmospheric and Oceanic Sciences & Institute of Atmospheric Sciences, Fudan University, Shanghai, China

^e Tianjin Meteorological Observatory, China Meteorological Administration, Tianjin, China

ARTICLE INFO

Keywords:

Sea Surface Temperature (SST)

Marine Heatwave (MHW)

Yellow Sea

Western Pacific subtropical high (WPSH)

Madden-Julian Oscillation (MJO)

ABSTRACT

Marine heatwaves (MHWs) are becoming more frequent and intense in many regions around the world. However, the MHWs over China's marginal seas and associated physical drivers are largely unknown. During August 2016, the Yellow Sea experienced the most intense MHW on record since 1982. Here, we used a set of high-resolution satellite data and reanalysis products to examine the characteristics of the MHW in August 2016 and analyze the potential influencing factors from atmospheric perspective. MHW was directly caused by greater-than-normal solar radiation and much weaker wind speeds which reduced upper oceanic mixing and caused substantial warming of the stratified surface layer. These anomalies were associated with an unusually fractured western Pacific subtropical high (WPSH) and the distinctly more active transmission of Madden-Julian Oscillation (MJO) eastward to the western Pacific in August 2016. The MJO triggered more frequent tropical cyclones, splitting the WPSH into two parts. The western segment of the WPSH combined with the continental high to form an abnormally positive geopotential height at the west of 120°E, causing strong subsiding flows at its east and extremely high solar radiation. An unambiguous cyclonic circulation anomaly in the lower troposphere, encompassing much of the northwestern Pacific, reduced the surface wind speed in the Yellow Sea. Therefore, MJO was critical to driving the extreme MHW in August 2016 in the Yellow Sea.

1. Introduction

Sea surface temperature (SST) has increased significantly across the globe in the past decades. A discrete period of prolonged anomalously warm water at a particular location could negatively impacted marine biodiversity and the provision of ecosystem services in all ocean basins (Hobday et al., 2016; Frölicher and Laufkötter, 2018). Such events may occur suddenly, anywhere in the world, and at any time of the year, which are classified as Marine Heat Waves (MHWs) by Hobday et al. (2016). In their definition, MHW is an abnormally warm water event with daily SSTs in a top range of historical baseline condition for a minimum of five consecutive days (Hobday et al., 2016). Due to their notable negative impact on marine ecosystem, MHWs have drawn much attention in recent years, like other terrestrial natural disasters.

Previous study suggests that driver mechanisms of MHWs are complex and multifarious, ranging from local dynamics to remote processes

via teleconnections in various spatial and temporal scales (Holbrook et al., 2019). These physical drivers include atmospheric forcing (Olita et al., 2007; Pearce and Feng, 2013; Chen et al., 2014), ocean stratification (Schaeffer and Roughan, 2017; Schlegel et al., 2017), cloud feedback (Myers et al., 2018), and advection of warm water through oceanic currents (Oliver et al., 2017), and also remote teleconnections associated with climatic modes of El Niño/La Niña (Pearce and Feng, 2013; Feng et al., 2013; Saleem et al., 2021), Indian Ocean Dipole (IOD) (Zhao et al., 2019), or Madden-Julian Oscillation (MJO) (Benthuyzen et al., 2018; Manta et al., 2018). For example, evidences have shown that the northeastern Pacific during boreal winter of 2013–2014 experienced an extreme MHW which was initiated by an unusually strong and persistent atmospheric pressure (Bond et al., 2015). Similarly, atmospheric pressure anomalies in association with ENSO that divert warm air poleward, weaken wind speeds, and slow the normal northward advection of cold water played a significant role in modulating

* Corresponding author.

E-mail address: mulin@szu.edu.cn (L. Mu).

MHWs in the South Pacific (Lee et al., 2010). Some nearshore MHWs may be triggered by weakening of coastal upwelling currents and weakened monsoon activity modulated by the MJO (Schlegel et al., 2017; Benthuysen et al., 2018). However, not all factors or drivers are important for each MHW. In fact, each event in a local region probably has its own constellation of drivers and needs to be investigated in detail.

In 2016, a quarter of the world's oceans experienced either the longest or most intense MHW since satellite records in 1982 (Oliver et al., 2017). As a semi-enclosed shelf sea in the middle-latitude of the Northern Hemisphere, the Yellow Sea (117° – 128° E, 32° – 39° N) supports much aquaculture, fishing activities and local marine organisms. In August 2016, it experienced an unprecedented MHW, which killed a large number of populations of varied species in part of the coastal and bay areas of South Korea (Gao et al., 2020) and contributed partly to the reproduction of severely harmful algae at the Yangtze River estuary and Yellow Sea (State Oceanic Administration of China, 2017). Over the last decade, there has been a surge in efforts to understand the genesis of MHWs across the globe which benefit for forecast and early warning. However, comparing to other regions, the physical processes of MHWs in the Yellow Sea are less understood. To date, there are no studies on the mechanisms of the MHW in August 2016, as well as the variations in MHWs in the Yellow Sea.

The purpose of this paper is to document MHWs in August in the Yellow Sea, examine the spatial and temporal pattern of the MHW in August 2016 and further investigate its links with potential physical drivers, including abnormality of atmospheric active centers and modes. This paper is organized as follows. Data and methods used are described in section 2. Section 3 shows the characteristics of the MHW in August 2016 in the context of history in the Yellow Sea. Section 4 investigates the causes of the record-breaking MHW from atmospheric perspective. Section 5 presents the summary and discussion.

2. Data and methods

2.1. Data

The NOAA daily Optimum Interpolation (OI) SST v2 covering 1 January 1982 to 31 December 2018 was used in our study (OISST v2, <https://www.esrl.noaa.gov/psd/>, Banzon et al., 2016). The dataset combines observations from different platforms, such as satellites, ships and buoys, and includes bias adjustment of satellite and ship observations to compensate for platform differences and sensor biases. OISST v2 is currently the longest data with high spatiotemporal resolution (0.25° latitude/longitude grid in daily) and has been widely used in identifying extreme oceanic events (Liao et al., 2015; Frölicher et al., 2018; Perkins-Kirkpatrick et al., 2019). Daily climatology was calculated from the 30 years (1983–2012) and smoothed with a method of centered-moving mean of 30 days.

Monthly mean geopotential heights, air temperature, zonal and meridional winds, cloud cover and vertical velocity fields from 1948 to 2018, are obtained from National Centers for Environmental Prediction/National Center for Atmospheric Research (NCEP/NCAR) reanalysis (<http://www.cdc.noaa.gov>, Kalnay et al., 1996). These data have the horizontal resolution of $2.5^{\circ} \times 2.5^{\circ}$ and have total of 17 vertical levels extending from 1000 to 10 hPa. Surface net downward solar shortwave radiation is derived from the newly released European Centre for Medium-Range Weather Forecasts Interim Reanalysis (ERA-Interim; Dee et al., 2011) with horizontal resolution of 1.0° , spanning from 1979 to 2018 (<https://apps.ecmwf.int/datasets/data/interim-full-mnonth/>). Depth-longitude profiles of sub-surface temperature anomalies were calculated from global ocean data assimilation system (GODAS) (Saha et al., 2006, <http://www.cpc.ncep.noaa.gov/products/GODAS/>). The Indian Ocean Dipole (IOD) index used is defined as the SST anomaly difference between the tropical western Indian Ocean (IO) (10° S– 10° N, 50° – 70° E) and southeastern IO (10° S– 0° , 90° – 110° E) (Saji et al., 1999).

Negative IOD (NIOD) is associated with warm SST and deep thermocline in the eastern IO, cool SST and shallow thermocline in the western IO.

The MJO is quantified by the daily Real-Time Multivariate MJO Index (RMM), which consists of the two leading principal components (PCs) of the field that combines average outgoing longwave radiation (OLR), zonal wind at 200, and zonal wind at 850 hPa from 15° S to 15° N (Wheeler and Hendon, 2004). The RMM index has eight phases numbered 1–8 that correspond to the eastward propagation of circulation and convection anomalies. Phases 1–4 correspond to MJO-related convection in the Indian Ocean, and phases 5–8 to MJO activity in the western Pacific. RMM values were obtained from the Australian Bureau of Meteorology (<http://www.bom.gov.au/climate/mjo/graphics/rmm.74toRealtime.txt>).

2.2. MHW definition and metrics

Normally, two types of definitions are used to identify the heat waves based on the absolute and relative threshold, respectively. For a better comparability with other regions and globe, a relative threshold for a MHW event which was defined by Hobday et al. (2016) and have been widely used was adopted in the study. MHW is identified as an anomalous, warm, discrete event prolonged for more than 5 consecutive days when the daily SST exceeds the daily 90th percentile threshold. The 90th percentile was calculated for each calendar day from all data within an 11-day window centered on the given day across the climatological period, and smoothed by 31-day moving average. Specially, two successive MHWs with a break of two days or less between them were considered a single continuous event. To quantitatively measure the MHWs, several metrics are used to describe the properties of MHWs, including duration (in days, number of consecutive days of percentile threshold exceedance of each MHW), the maximum intensity (in $^{\circ}$ C; maximum SST anomaly in the duration of an event), the cumulative mean intensity (in $^{\circ}$ C days; the mean intensity multiplied with the duration of an event), and the spatial extent (in km^2 , area over which MHW detected) (more details see "Method" in Hobday et al., 2016).

With ongoing anthropogenic warming, there is the expectation that MHWs will become more intense over time. Here, we also calculated the severity of each MHW using a simple categorization scheme by Hobday et al. (2018). Multiples of the 90th percentile differences from the mean climatology value categorizes the severity of an MHW and allowed for the identification of the more extreme events. MHWs are categorized as moderate when the daily SST is above the 90th percentile of the climatological distribution for 5 days or longer (Category I); the subsequent categories are defined with respect to the difference between the SST and the climatological average: strong (Category II), severe (Category III), or extreme (Category IV), if that difference is, respectively, more than two, three or four times the difference between the 90th percentile and the climatological distribution average. Based on this scheme, we can compare events in a consistent way and further enhance public awareness. MHWs can be calculated using the freely available R-code package developed by Hobday et al. (2016) (<https://github.com/cran/RmarineHeatWaves>).

2.3. Probability density functions (PDFs) and generalized extreme value (GEV)-fit

Probability density functions (PDFs) are calculated using the daily SST anomalies in august for two 16-year time periods; 1982–1997 and 2003–2018. Statistical characteristics of the PDFs, such as the higher moments (mean, variance, skewness and kurtosis), are also calculated. The occurrence probabilities of SST anomalies exceeding 90th and 99th percentile climatology are determined by computing the probability for SST anomalies above 90th and 99th percentile climatology. The generalized extreme value (GEV)-fit distribution is used when estimating the PDFs. GEV distribution is widely employed in the environmental sciences for modelling extremes. The GEV distribution unites the Gumbel,

Fréchet and Weibull distributions into a single family to allow a continuous range of possible shapes.

Based on the extreme value theory that derives the GEV distribution, we can fit a sample of extremes to the GEV distribution to obtain the parameters that best explains the probability distribution of very rare or the extremes. In our present work, the observed August SST anomalies are, respectively, fitted to the GEV distribution. From the fitted distribution, we can estimate how often the August 2016 extreme heat occur with a certain return level. The return value is defined as a value that is expected to be equaled or exceeded on average once every interval of time (T) (with a probability of $1/T$).

3. Marine heatwaves in the Yellow Sea

3.1. MHW in August 2016 in the context of history

The Yellow Sea experienced remarkably high temperature in August 2016, with a peak magnitude of over 2.2°C at the center (~ 2.0 standard deviations above normal) (Fig. 1(a)). For the study region ($32^{\circ}\text{--}39^{\circ}\text{N}$, $117^{\circ}\text{--}128^{\circ}\text{E}$), August 2016 (black dot) is the warmest month ever recorded back to 1982 (Fig. 1(b)). And the observed SST in August 2016 corresponds to a 1-in-140-years event, based on the GEV fit (Fig. 1c). Applying the MHW definition, we found that the Yellow Sea region was in a continuous MHW from 5 to 26 August 2016 (Fig. 1(d)), and 73% days were classified as Category II. Moreover, 75 regional MHWs were

further identified in 1982–2018 (Fig. 1(d)), with a total of 977 MHW days (sum days of the durations of the 75 MHWs). The MHW in August 2016 was the most intensive, with the maximum intensity of 3.54°C (Fig. 1(d)) (Table 1). In the following text, the MHW was named based on its location and year, i.e., Yellow Sea 2016.

Using the regional daily SST anomalies during August, changes in temperature distribution in two 16-year subsets; 1982–1997 and 2003–2018 were investigated (Fig. 2). For this region, the mean

Table 1

Ten MHWs classified into Category II and associated heatwave metrics. The entry for each event lists the date of peak maximum intensity, the maximum intensity (I_{\max} , $^{\circ}\text{C}$), the duration of the event (days), and the proportion of time spent in each of Category II over the whole duration of the event (P_{strong} , %). The MHW focused in our work is in bold.

Categorization	No.	Peak Data	I_{\max}	Duration	P_{strong}
Category II (Strong)	1	Aug 14 2016	3.54	22	73%
	2	28 Feb 2007	2.41	26	35%
	3	25 Apr 2014	2.79	17	24%
	4	21 May 2017	2.70	21	24%
	5	9 Aug 2018	2.85	18	22%
	6	20 Jul 2017	3.14	61	18%
	7	14 Aug 2006	2.74	11	18%
	8	9 Aug 2013	2.45	29	14%
	9	9 Apr 2009	2.47	16	13%
	10	4 Dec 2004	2.38	38	5%

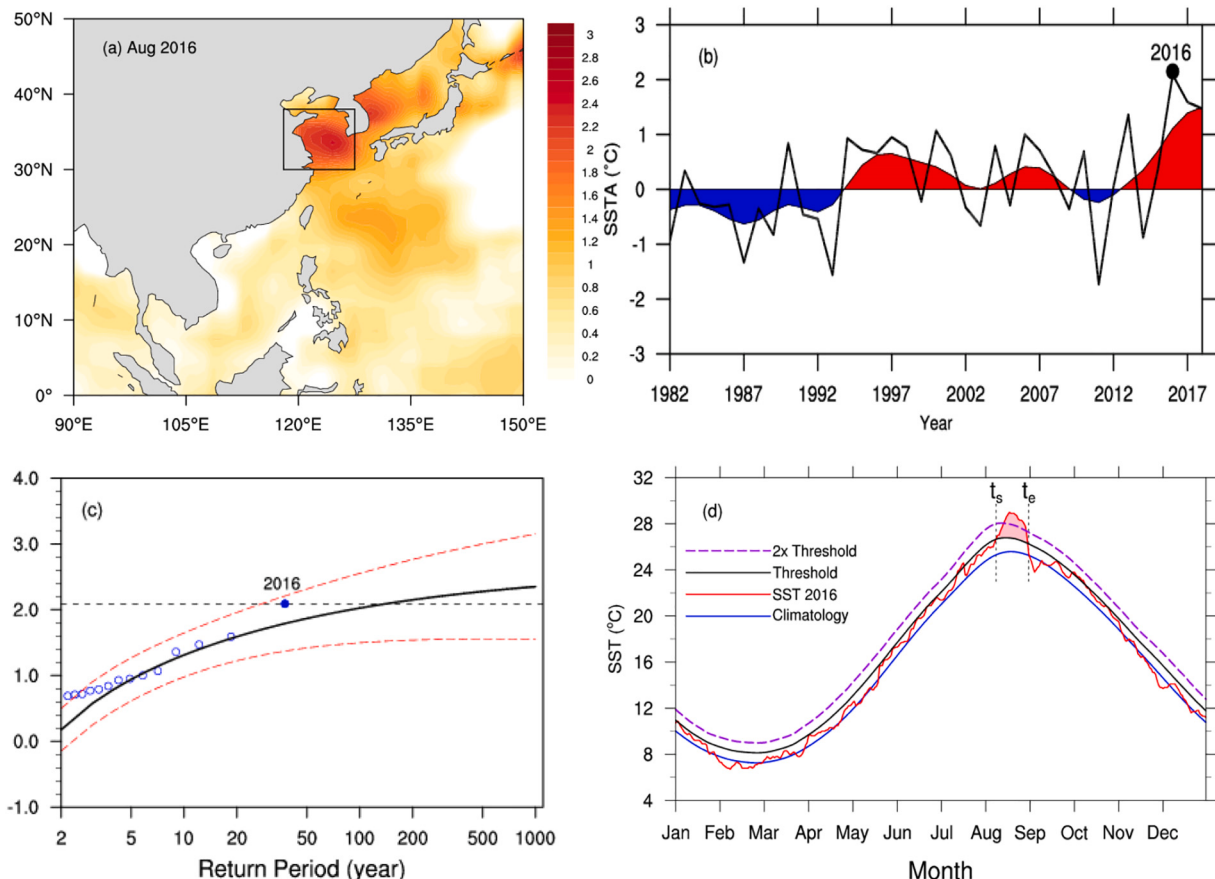


Fig. 1. (a) Sea surface temperature (SST) anomalies ($^{\circ}\text{C}$) in the China Seas for August 2016. Anomalies are calculated relative to the mean from 1983 to 2012. Rectangle indicates the domain of the study ($117^{\circ}\text{--}128^{\circ}\text{E}$, $32^{\circ}\text{--}39^{\circ}\text{N}$). (b) Monthly SST anomalies for the monthly of August averaged over the Yellow Sea denoted by the black box in Fig. 1a from 1982 to 2018. The smoother shaded area is the 9-yr running mean. (c) Generalized Extreme Value (GEV) fit (black solid line) of observed August SSTs with 95% confidence intervals (red dashed line). The blue dots are the observed August SSTs from 1982 to 2018. The black dashed line denotes the year 2016. (d) Daily mean SST anomalies averaged over the Yellow Sea from 1 January to 30 December 2016 (red line), with the category II for each day (purple line). The start time (t_s) and end time (t_e) of the Yellow Sea 2016 also shown here. The grey and blue lines indicate the 90th percentile threshold and climatological mean, respectively. (For interpretation of the references to colour in this figure legend, the reader is referred to the web version of this article.)

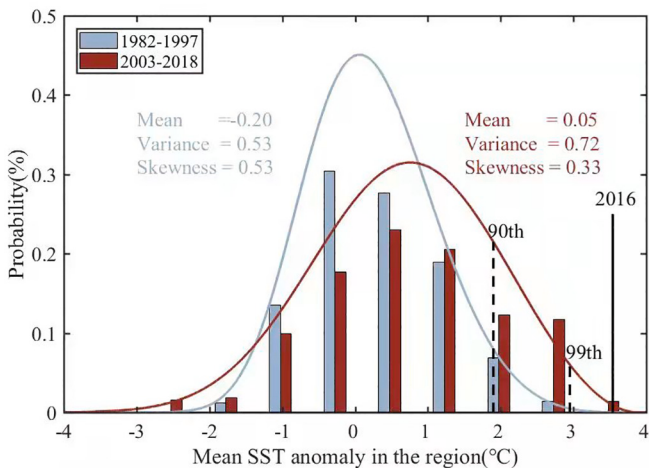


Fig. 2. Histograms and GEV-fit probability density functions (PDFs) of August SST anomalies of the region (117° – 128° E, 32° – 39° N) are presented for the periods 1982–1997 (blue bars and blue line) and 2003–2018 (red bars and red line). Statistics related to the shape, scale, and location parameters (mean, variance, skewness) are also shown. The black dashed lines represent 90th percentile and 99th percentile of climatological period (1983–2012). The thick black line is the observed maximum SST anomaly of MHW 2016. (For interpretation of the references to colour in this figure legend, the reader is referred to the web version of this article.)

anomalies increased by 0.25° C, with a clear shift toward warmer-side in the latter period. An increase in variance from 0.53 to 0.72 alone also increased the probability of extreme events. Meanwhile, there was a change in asymmetry toward the hotter part (skewness transfers from 0.26 to 0.33) and the distribution is becoming wider and lower during 2003–2018 (kurtosis transfers from 0.81 to 0.66). The changing variance and shape of distribution have had a greater impact on the hot SST anomalies than cool SST anomalies. And these changes notably increased the occurrence probability of hot extremes. The occurrence probability of SST anomalies exceeding 90th percentile is 2.8% during 1982–1997 and it is up to 15.5% during 2003–2018. The occurrence probability of exceeding 99th percentile also notably transferred from 0.16% to 4.0%. Since the magnitude of the MHW 2016 lies at the far warm-end tail of PDF, natural climate variability has also clearly increased the occurrence probability of the event in August 2016, in addition to anthropogenic warming or multidecadal modulations (Donat and Alexander, 2012; Gao et al., 2020). Thus, a well understand of the natural physical mechanism can benefit for the prediction of MHWs in the Yellow Sea.

4. Drivers of the record-breaking MHW from atmospheric perspective

From the perspective of predictability of individual MHW event, this work attempts to address the role from natural factors in the following parts, with the focus on the possible relationship between the SST anomalies and the atmospheric circulation modes.

4.1. Atmospheric conditions before and during the MHW

The anomaly patterns, including geopotential height (GHT), air temperature (AT), sea level pressure (SLP), 10 m horizontal wind and solar radiation, are shown in Figs. 3 and 4. In July 2016, before the beginning of the MHW in August 2016, above-normal temperature and drier air were localized over the mainland China (Fig. 3(a) and (c)). Anticyclonic anomalies at (30° – 50° N, 100° – 130° E) were induced by the westward extension of the western Pacific subtropical high (WPSH) which penetrated through the troposphere from surface to tropopause

(Figs. 3(e) and 4(a)). Weak sinking motion dominated in west of the mainland China, while rising motion dominated at the Yellow Sea (Fig. 3(g)). The near-surface atmospheric conditions showed a stronger than normal SLP in the Yellow Sea. This higher atmospheric pressure brought southerly wind anomalies from the East China Sea (ECS) to the Yellow Sea (Fig. 4(c)). Under this condition, warming waters from the ECS arriving at the Yellow Sea would contribute to warming in the region. However, due to the weak sinking motion and larger cloudiness (not shown), there were smaller solar radiation in July 2016. Consequently, the positive SST anomalies were much weaker in July than those in August 2016 (Figure omitted).

Atmospheric anomalous conditions in August 2016 experienced notable changes comparing with those in July 2016. High-temperature and low-relative humidity anomalies extended to the upper troposphere, suggesting a much warmer and drier air column over the region of interest (Fig. 3(b), Fig. 3(d)). There were huge positive GHT anomalies on the west side of the Yellow Sea and strong negative anomalies on its east side (Fig. 3(f)). Anomalous subsidence appeared over the Yellow Sea, with a center around the 500-hPa level at 130° E (Fig. 3(h)). This subsiding flow, as well as the warm and dry conditions in the study region, led to less cloud cover which increased solar radiation reached at the surface, with anomalous value exceeding 60 W m^{-2} (Fig. 4(f)). In particular, the regional average cloudiness over the Yellow Sea in August 2016 is the least since 1982 (Figure not shown) and the solar radiation has ranked as the second-largest (66.8 W m^{-2}), only next to the year of 2013 (68.4 W m^{-2}). The Yellow Sea was thus warmed efficiently by the strong solar shortwave radiation.

For the near-surface patterns, there were a higher-than-normal SLP in the western of the Yellow Sea and a lower-than-normal SLP in the eastern Yellow Sea. The presence of the anticyclonic and cyclonic anomalies induced a northeasterly anomaly in this region (Fig. 4(d)). Wind speeds were around 1.4 m/s lower than normal in the Yellow Sea. The weak wind condition led to an intense stratification of sea water that was unable to break because there was not enough vertical mixing (Manta et al., 2018). The strong solar radiation could be trapped over the thinner mixed layer (ML) and thus efficiently heated SST. The GODAS sub-surface ocean temperature pattern in August 2016 indicated a very shallow anomaly profile, mainly confined to the upper 20 m (Fig. 4(h)). Meanwhile, northeasterly winds in August 2016 inhibit the horizontal warm water from the ECS (normally there are southeasterly winds in August in the study region). This mechanism contrasts with the 2015/16 MHW reported by Oliver et al. (2017), where horizontal oceanic heat advection by the East Australian Current was identified to be the important driver. The shortwave radiation acted predominantly as a forcing of the regional SST anomalies of the Yellow Sea in August 2016, under the condition of very shallow ML. Therefore, the Yellow Sea 2016 was associated with greater-than-normal solar radiation and weaker surface winds which were attributable to the abnormal atmospheric circulations discussed above. And these anomalies are likely linked to the rapid change of the WPSH, which we will examine in following section.

4.2. Western Pacific subtropical high

Generally, the WPSH is regarded as the key anticyclone system for the climate variability in the China Seas (Pei et al., 2017). Fig. 5 displays the monthly mean GHT at 500 hPa (Z500) in July and August 2016, with 5870 gpm contour denoting the domain of the WPSH. In July 2016, the region encompassed by 5870 gpm was zonally elongated with the westernmost ridge located at 110° E (Fig. 5(a)). However, the WPSH during August 2016 split into two parts (Fig. 5(b)). The eastern segment weakened and retreated rapidly to the east of 150° E and the western segment combined with the continental high to form an abnormally higher geopotential height at the west of 120° E (Fig. 5(d)). The powerful continental high persistently dominated Eastern China and East Asian Summer Monsoon (EASM) suddenly became stronger (Yuan et al.,

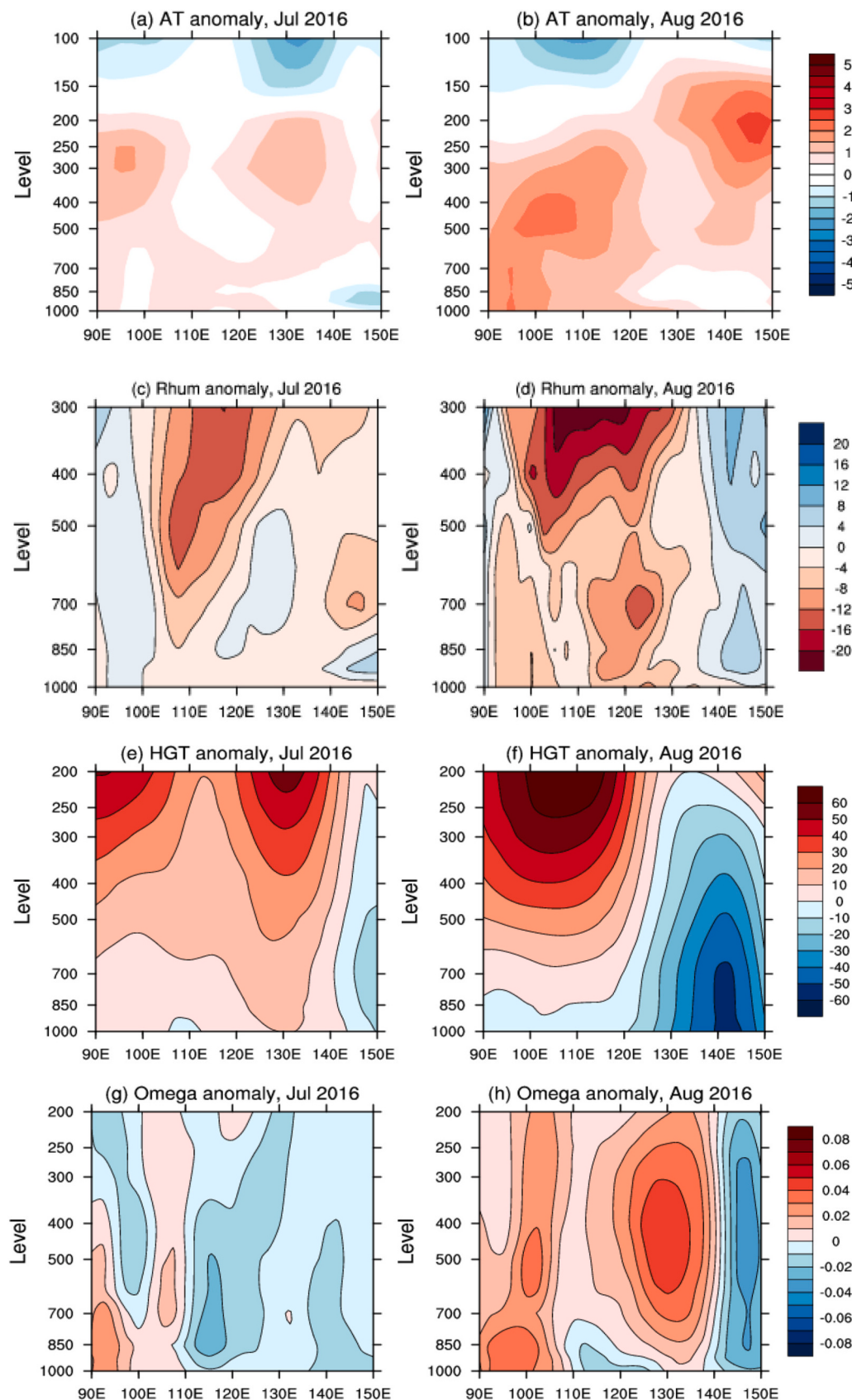


Fig. 3. Longitude-height cross section of anomalies (colour shading) of air temperature (unit: °C) in July (a) and August (b) 2016, relative humidity (unit: %) in July (c) and August (d) 2016 (negative value means dry condition), geopotential height (unit: gpm) in July (e) and August (f) 2016, vertical velocity (omega, unit: Pa/s) in July (g) and August (h) 2016, along 33°N (positive value means sinking motion).

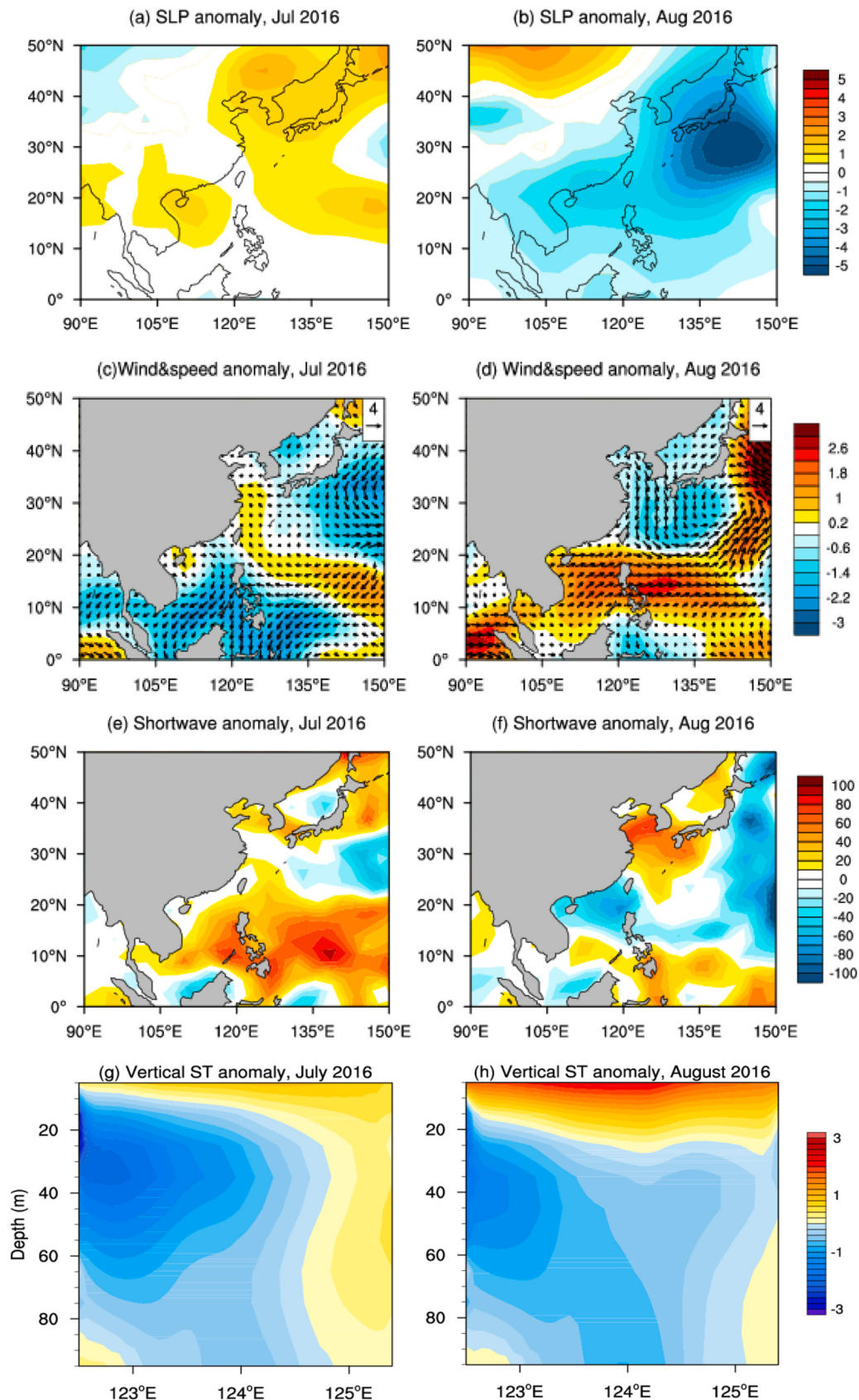


Fig. 4. Sea level pressure anomalies (unit: hPa) in July (a) and August (b) 2016; Winds (arrows)& wind speed anomalies (colour shaded) (unit: m/s) in July (c) and August (d) 2016; Shortwave radiation anomalies in July (e) and August (f) 2016, denote net shortwave heat fluxes (W/m^2), defined as positive downward (into the ocean); Vertical sections of sea water temperature anomalies (unit: $^{\circ}\text{C}$) along from $(122.5^{\circ}\text{E}, 30^{\circ}\text{N})$ to $(125.4^{\circ}\text{E}, 36^{\circ}\text{N})$ in July (g) and August (h) 2016. Anomalies are calculated relative to the mean from 1983 to 2012.

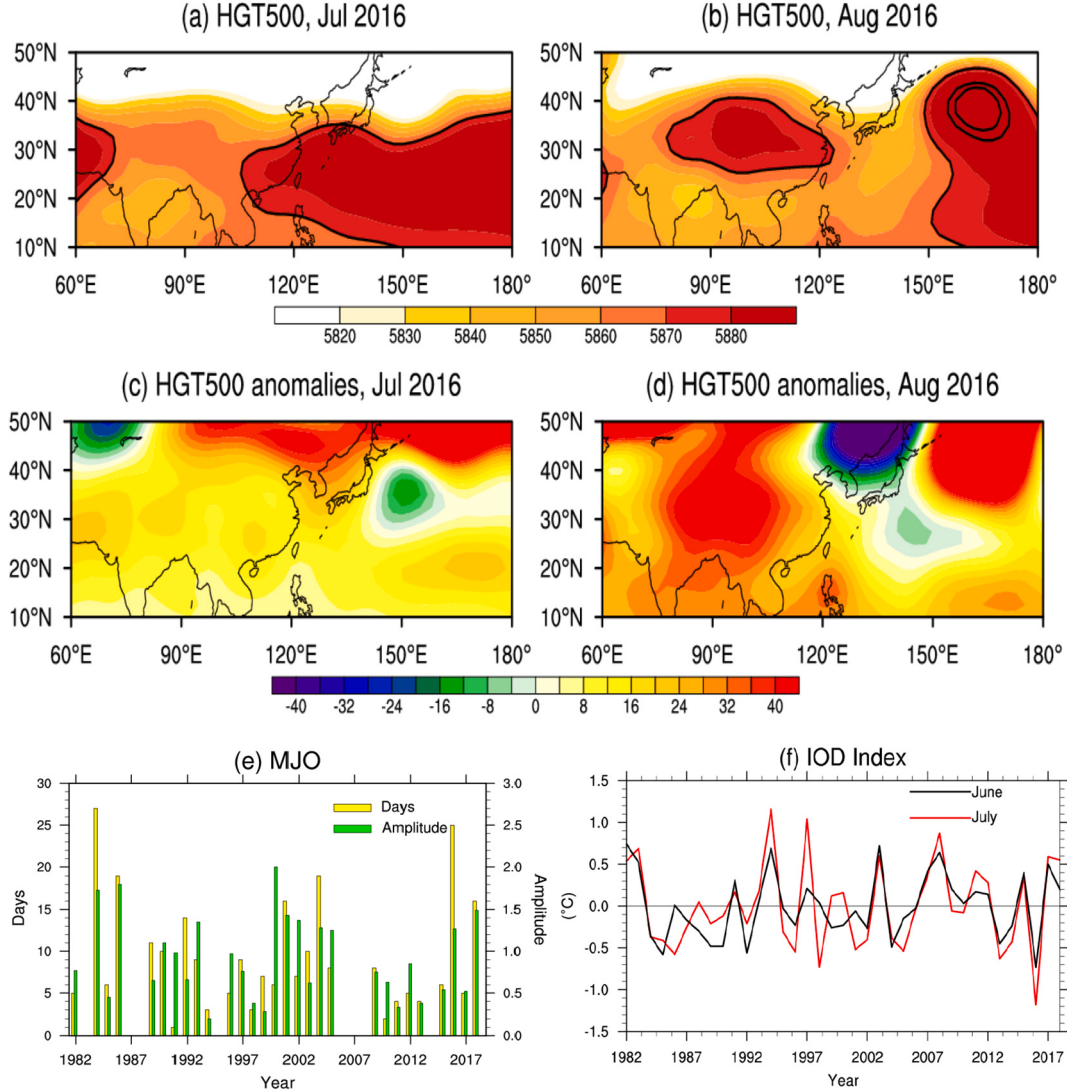


Fig. 5. The 500-hPa geopotential height in July (a) and August (b) 2016, the WPSH represented by black 5870 gpm contour; The 500 hPa geopotential height anomalies in July (c) and August (d) 2016 (units: gpm). The time series of MJO days (yellow bars) and amplitude (green bars) in Phases 6 and 7 in August from 1982 to 2018 (e), and IOD index in June (black line) and July (red line) from 1982 to 2018 (f). (For interpretation of the references to colour in this figure legend, the reader is referred to the web version of this article.)

2017). The abnormally continental high pressure was responsible for the subsiding flow in its east, which led to the regional warm and dry conditions above the Yellow Sea. Meanwhile, a strong negative anomalous GHT with the center located at (30°N, 140°E) and an anomalous cyclonic circulation (Fig. 3(f) and Fig. 4(d)). The low troposphere in the eastern Yellow Sea was controlled by abnormally cyclonic circulation which can induce a northerly anomaly and weaken southerly flow in the Yellow Sea and thus, led to a more intense stratification and weaker vertical mixing.

It is important to make clear what triggered the WPSH suddenly to split in August 2016. In a sharp contrast to the first half of the year when tropical cyclone activity was suppressed, seven typhoons formed in the northwestern Pacific basin in August 2016 (Blunden, 2017). Four of these made landfall in rapid succession in Japan. It was the largest number of typhoon landfalls on Japan in a single month since records began in 1951. The frequent typhoons were associated with the far eastward WPSH and large cyclonic circulation anomalies in the lower troposphere (Blunden, 2017; Sun et al., 2017).

In August 2016, the southwesterly monsoonal surge associated with the strong MJO event was strengthened, forming a vigorous convection belt centered roughly at 15°N and promoting the TC formations and

development (Chen and Wang, 2018). The daily monitoring of MJO exponential phase diagrams shows that MJO spread eastward to the Western Pacific (Phases 6–7) in August 2016. Normally, in August of the following year of moderate or strong El Niño, the MJO Phases 6–7 tend to be less active and weaker. However, much more active MJO occurred in August 2016, which is seldom seen in history. The MJO Phases 6–7 lasted for 25 days from 5 to 29 August without interruption, exceeding the climatic average (7.4 days) by nearly 18 days, which was the second-longest since 1982, only next to 1984 (27 days) (Fig. 5(e)). The average amplitude of MJO Phase 6–7 in August 2016 was 1.27 which was also stronger than normal (0.72). The MJO is widely acknowledged for its ability to modulate Northwest Pacific TCs (Huang et al., 2011; Fowler and Pritchard, 2020). Previous study showed that in the strong MJO period, the total typhoon genesis cases during phases 6 and 7 were 2 times of those during phases 2 and 3 (Pan et al., 2010). Thus, the much more active MJO in August 2016 is an important reason for the abnormal activity of typhoons in the northwestern Pacific, which led to the splitting of the WPSH, following with the weakened and eastward retreated subtropical high (Yuan et al., 2017).

The MJO is a leading intra-seasonal climate mode of tropical convective variability, originating in the western IO. The anomalous

warm water in the southeastern IO and low-level westerly anomalies over the equatorial central IO favored the eastward movement of MJO (Yuan et al., 2014). The basin wide warming was observed from January to April 2016. In May 2016, the intra-seasonal disturbances induced the early subsurface cooling over the western IO and initiated the negative IOD in 2016 (Lu et al., 2018). Subsequently, IOD event rapidly developed in the summer of 2016. It is the strongest IOD in negative phase since 1982 according to OISST v2, with IOD indices in June and July reaching -0.73°C and -1.18°C , respectively (Fig. 4(f)). The correlations between IOD index and the accumulated days of MJO in phases 6–7 are significant in June ($r = -0.41$, exceeding 99% confidence level) and July ($r = -0.36$, exceeding 95% confidence level), respectively.

In summary, the Yellow Sea 2016 was closely linked to the rapid change of the WPSH in August 2016 which split into two isolated parts. The active tropical cyclones and MJO over the West Pacific played a crucial role in the splitting of WPSH, which may be related to the tropical driver — rapidly developing of the strong negative IOD from May to August 2016.

5. Conclusions and discussion

From 5 to 26 August 2016, the Yellow Sea experienced the most intense MHW on the satellite record (1982–2018). We analyzed the drivers of the record-breaking MHW from atmospheric variability perspective and further explored a possibility that MHWs in the middle-latitude could also be related to tropical intra-seasonal oscillations and extratropical atmospheric variability modes. A schematic representation of the formation of this MHW is shown in Fig. 6. The separation of the WPSH into two independent components of eastern and western segments promoted the formation and development of the MHW in the Yellow Sea in August 2016. The eastern segment weakened and retreated rapidly to the east of 150°E and the western segment combined with the continental high to form an abnormally strong geopotential

height at the west of 120°E . This sandwich-like structure might be partly caused by the more active MJO and typhoons. The strong MJO spread eastward to the western Pacific Ocean and the abnormally active tropical cyclones were generated. The anomalous sinking motion over the east of the continental high pressure could cause clearer sky and enhance the solar radiation reaching at the surface, leading to greater heating. The cyclonic circulation anomalies over the west northern Pacific were associated with suppressed wind speeds of southerly in the study region. The low wind speeds reduced the upper ocean mixing, which caused severe warming of the stratified surface layer of the Yellow Sea. Our work displayed that the increased solar radiation, weaker wind anomalies, and reduced vertical mixing were direct factors for the warming event. An unusually fractured WPSH and the distinctly more active transmission of MJO eastward to the western Pacific played a significant and critical role in leading these anomalous heat and wind.

Furthermore, our study showed that the remote influences, and the oceanic or atmospheric teleconnection processes in tropical or extra-tropical areas, appears to be important modulators for the occurrence of such heat extremes. Populations residing near the warm limit of given species, such as abalones, sea cucumbers, scallops, etc., are particularly vulnerable to extreme warming events. These findings may be beneficial to studies on the potential predictability of regional MHWs and setting up early warning systems which can help in increasing the preparedness of the fishery and other marine sectors to the impacts of severe MHWs.

MHWs can be triggered by a whole range of factors, and not all factors are equally important for each event. There remains a complex physical mechanism between large-scale atmospheric and oceanic systems and the occurrence of the MHWs. These will become more complex by the influence of local and global processes, including the Yangtze River discharge, ocean advection, aerosol, and sea water upwelling (Lima and Wethey, 2012; Tan and Cai, 2018; Moon et al., 2019; Gao et al., 2020). Moon et al. (2019) pointed out that the shallow ML over the Yellow Sea resulted from Yangtze River discharge-induced salinity

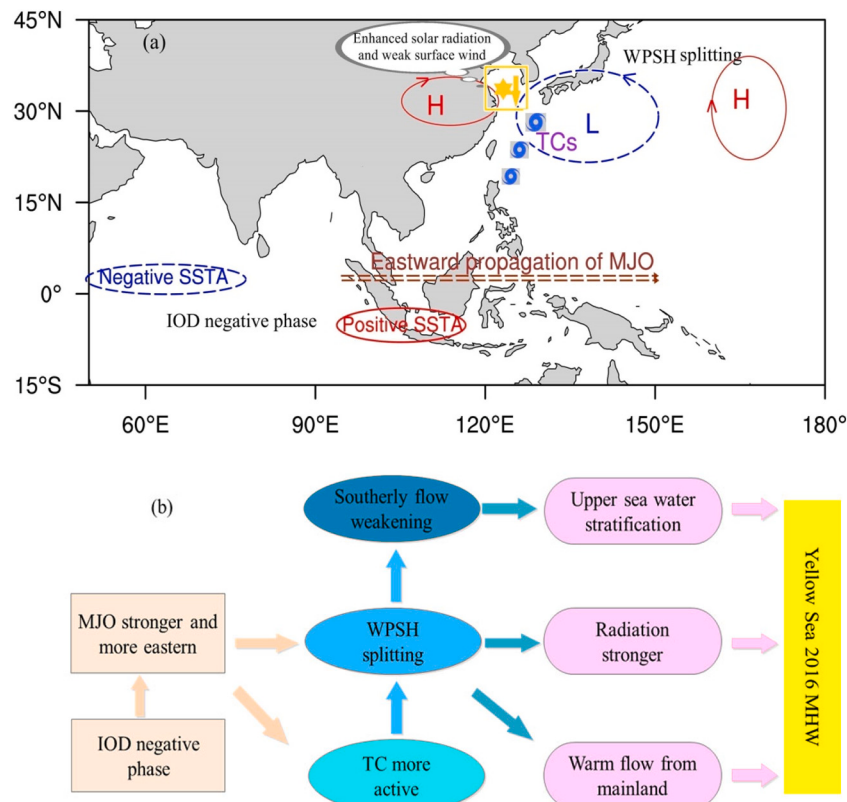


Fig. 6. Schematic representation of the atmospheric circulation associated with the MHW in the Yellow Sea in the August 2016 (a) and possible mechanisms (b). (For interpretation of the references to colour in this figure legend, the reader is referred to the web version of this article.)

stratification and led to barrier layer formation between the ML and the layer below ML. This enhanced barrier layer restricts the vertical heat exchanges and the SST warming can be strengthened by trapping heat in the shallower ML. Determining these local causal factors is still an area of ongoing researches. As an additional critical point, various climate modes, i.e., ENSO, IOD, Pacific Decadal Oscillation (PDO), can act as local MHW mechanisms via atmospheric and oceanic pathways. It has been known to the public that such ENSO teleconnections can be amplified by local air-sea feedback processes or work in concert with stochastic local weather conditions (Yao and Wang, 2021). These analyses should be performed in future studies.

In the present work, we focus on the drivers of the record-breaking MHW from atmospheric perspective. We did not explore the attributions of this extreme event, though there are considerable analyses found that anthropogenically caused climate change was an attribution to extreme events globally. In the following work, we will try to explain the occurring of MHWs in the Yellow Sea from a climate perspective.

Declaration of Competing Interest

The authors declare that they have no known competing financial interests or personal relationships that could have appeared to influence the work reported in this paper.

Acknowledgments

This study was supported by the Natural Science Foundation of China (42170617), the Shenzhen Fundamental Research Program (JCYJ20200109110220482), the Special Project for Introduced Talents Team of Southern Marine Science and Engineering Guangdong Laboratory (Guangzhou) (GML2019ZD0604), the National Key Research and Development Program of China (2018YFA0605600).

References

- Banzon, V., Smith, T.M., Chin, T.M., Liu, C., Hankins, W., 2016. A long-term record of blended satellite and in situ sea-surface temperature for climate monitoring, modeling, and environmental studies. *Earth Syst. Sci. Data* 8, 165–176.
- Benthuyzen, J.A., Oliver, E.C.J., Feng, M., Marshall, A.G., 2018. Extreme marine warming across tropical Australia during austral summer 2015–2016. *J. Geophys. Res. Oceans* 2, 1301–1326.
- Blunden, J., 2017. State of the climate in 2016. *Bull. Am. Meteorol. Soc.* 98 (8), Si–S277.
- Bond, N.A., Cronin, M.F., Freeland, H., Mantua, N., 2015. Causes and impacts of the 2014 warm anomaly in the NE Pacific. *Geophys. Res. Lett.* 42 (9), 3414–3420.
- Chen, K., Gawarkiewicz, G.G., Lentz, S.J., Bane, J.M., 2014. Diagnosing the warming of the northeastern U.S. coastal ocean in 2012: a linkage between the atmospheric jet stream variability and ocean response. *J. Geophys. Res. Oceans* 119, 218–227.
- Chen, G., Wang, K., 2018. Why is the tropical cyclone activity over the Western North Pacific so distinct in 2016 and 1998 following super El Niño event? *J. Meteorol. Soc. Japan* 96 (2), 97–110.
- Dee, D.P., Uppala, S.M., Simmons, A.J., Berrisford, P., Poli, P., Kobayashi, S., Andrae, U., Balmaseda, M.A., Balsamo, G., Bauer, D.P., Bechtold, P., 2011. The ERA-interim reanalysis: configuration and performance of the data assimilation system. *Q. J. R. Meteorol. Soc.* 137 (656), 553–597.
- Donat, M.G., Alexander, L.V., 2012. The shifting probability distribution of global daytime and night-time temperatures. *Geophys. Res. Lett.* 39 (14), L14707.
- Feng, M., McPhaden, M.J., Xie, S.P., Hafner, J., 2013. La Niña forces unprecedented Leeuwin current warming in 2011. *Sci. Rep.* 3 (2013), 1277.
- Fowler, M.D., Pritchard, M.S., 2020. Regional MJO modulation of Northwest Pacific tropical cyclones driven by multiple transient controls. *Geophys. Res. Lett.* 47 (11), e2020GL087148.
- Frölicher, T.L., Laufkötter, C., 2018. Emerging risks from marine heat waves. *Nat. Commun.* 9 (1), 650.
- Frölicher, T.L., Fischer, E.M., Gruber, N., 2018. Marine heatwaves under global warming. *Nature* 560, 360–364.
- Gao, G., Marin, M., Feng, M., Yin, B., Yang, D., Feng, X., Ding, Y., Song, D., 2020. Drivers of marine heatwaves in the East China Sea and the South Yellow Sea in three consecutive summers during 2016–2018. *J. Geophys. Res. Oceans* 125 (8), 1–19.
- Hobday, A.J., Alexander, L.V., Perkins, S.E., Smale, D.A., Straub, S.C., Oliver, E.C.J., Benthuyzen, J.A., Burrows, M.T., Donat, M.G., Peng, M., Holbrook, N.J., Moore, P.J., Scannell, H.A., Sen Gupta, A., Wernberg, T., 2016. A hierarchical approach to defining marine heatwaves. *Prog. Oceanogr.* 141, 227–238.
- Hobday, A.J., Oliver, E.C.J., Sen Gupta, A., Benthuyzen, J.A., Burrows, M.T., Donat, M.G., Holbrook, N.J., Moore, P.J., Thomsen, M.S., Wernberg, T., Smale, D.A., 2018. Categorizing and naming marine heatwaves. *Oceanography* 31 (2), 162–173.
- Holbrook, N.J., Scannell, H.A., Sen Gupta, A., Benthuyzen, J.A., Feng, M., Oliver, E.C.J., Alexander, Lisa V., Burrows, M.T., Donat, M.G., Hobday, A.J., Moore, P.J., Perkins-Kirkpatrick, S.E., Smale, D.A., Straub, S.C., Wernberg, T., 2019. A global assessment of marine heatwaves and their drivers. *Nat. Commun.* 10, 2624.
- Huang, P., Chou, C., Huang, R., 2011. Seasonal modulation of tropical intraseasonal oscillations on tropical cyclone geneses in the Western North Pacific. *J. Clim.* 24 (24), 6339–6352.
- Kalnay, E., Kanamitsu, M., Kistler, R., Collins, W., Deaven, D., Gandin, L., Iredell, M., Saha, S., White, G., Woollen, J., Zhu, Y., Leetmaa, A., Reynolds, R., Chelliah, M., Ebisuzaki, W., Higgins, W., Janowiak, J., Mo, K.C., Ropelewski, C., Wang, J., Jenne, R., Joseph, D., 1996. The NCEP/NCAR 40-year reanalysis project. *Bull. Am. Meteorol. Soc.* 77 (1996), 789–799.
- Lee, T., Hobbs, W.R., Willis, J.K., Halkides, D., Fukumori, I., Armstrong, E.M., Hayashi, A.K., Timothy Liu, W., Patzert, W., Wang, O., 2010. Record warming in the South Pacific and western Antarctica associated with the strong Central-Pacific El Niño in 2009–10. *Geophys. Res. Lett.* 37 (19), 1–6.
- Liao, E.H., Lu, W.F., Yan, X.H., Jiang, Y.W., Kidwell, A., 2015. The coastal ocean response to the global warming acceleration and hiatus. *Sci. Rep.* 5, 16630.
- Lima, F.P., Wethay, D.S., 2012. Three decades of high-resolution coastal sea surface temperatures reveal more than warming. *Nat. Commun.* 3, 704.
- Lu, B., Ren, H.L., Scaife, A.A., Wu, J., Dunstone, N., Smith, D., Wan, J.H., Eade, R., MacLachlan, C., Gordon, M., 2018. An extreme negative Indian ocean dipole event in 2016: dynamics and predictability. *Clim. Dyn.* 51 (1–2), 89–100.
- Manta, G., Mello, S. de, Trinchin, R., Badagian, J., Barreiro, M., 2018. The 2017 record marine heatwave in the Southwestern Atlantic Shelf. *Geophys. Res. Lett.* 45 (22), 12449–12456.
- Moon, J.H., Kim, T., Son, Y.B., Hong, J.S., Lee, J.H., Chang, P.H., Kim, S.K., 2019. Contribution of low-salinity water to sea surface warming of the East China Sea in the summer of 2016. *Prog. Oceanogr.* 175 (JUL-AUG.), 68–80.
- Myers, T.A., Mechoso, C.R., Cesana, G.V., Deflorio, M.J., Waliser, D.E., 2018. Cloud feedback key to marine heatwave off Baja California. *Geophys. Res. Lett.* 45, 4345–4352.
- Olita, A., Sorgente, R., Natale, S., Gabersek, S., Ribotti, A., Bonanno, A., Patti, B., 2007. Effects of the 2003 European heatwave on the Central Mediterranean Sea: surface fluxes and the dynamical response. *Ocean Sci.* 3 (2), 273–289.
- Oliver, E.C.J., Benthuyzen, J.A., Bindoff, N.L., Hobday, A.J., Holbrook, N.J., Mundt, C.N., Perkins-Kirkpatrick, Sarah E., 2017. The unprecedented 2015/16 Tasman Sea marine heatwave. *Nat. Commun.* 8 (2017), 16101.
- Pan, J., Li, C.Y., Song, J., 2010. The modulation of Madden-Julian oscillation on typhoons in the northwestern Pacific Ocean. *Chin. J. Atmos. Sci.* 34 (6), 1059–1070 (in Chinese).
- Pearce, A.F., Feng, M., 2013. The rise and fall of the “marine heat wave” off Western Australia during the summer of 2010/2011. *J. Mar. Syst.* 111–112s, 139–156.
- Pei, Y.H., Liu, X.H., He, H.I., 2017. Interpreting the sea surface temperature warming trend in the Yellow Sea and East China Sea. *Sci. China Earth Sci.* 60 (8), 1558–1568.
- Perkins-Kirkpatrick, S.E., King, A.D., Coughon, E.A., Grose, M.R., Oliver, E.C.J., Holbrook, N.J., Pourashgar, F., 2019. The role of natural variability and anthropogenic climate change in the 2017/18 Tasman Sea marine heatwave. *Bull. Am. Meteorol. Soc.* 100 (1), 105–110.
- Saha, S., Nadiga, S., Thiaw, C., Wang, J., Wang, W., Zhang, Q., van den Dool, H.M., Pan, H., Moorthi, S., Behringer, D., Stokes, D., White, G.R., Lord, S., Ebisuzaki, W., Peng, Pen-Jui, Xie, S.P., 2006. The ncep climate forecast system. *J. Clim.* 19, 3483–3517.
- Saji, N.H., Goswami, B.N., Vinayachandran, P.N., Yamagata, T., 1999. A dipole mode in the tropical Indian Ocean. *Nature* 401, 360–363.
- Saleem, F., Zeng, X., Hina, S., Omer, A., 2021. Regional changes in extreme temperature records over Pakistan and their relation to Pacific variability. *Atmos. Res.* 250, 105407.
- Schaeffer, A., Roughan, M., 2017. Subsurface intensification of marine heatwaves off southeastern Australia: the role of stratification and local winds. *Geophys. Res. Lett.* 44, 5025–5033.
- Schlegel, R.W., Oliver, E.C.J., Sarah, P.K., Andries, K., Smit, A.J., 2017. Predominant atmospheric and oceanic patterns during coastal marine heatwaves. *Front. Mar. Sci.* 4, 323.
- State Oceanic Administration of China, 2017. China Marine Disaster Bulletin. China Government Network. <http://www.mnr.gov.cn/sj/jfw/hy/gbgg/zghyzhgb/>.
- Sun, Y., Zhong, Z., Li, T., Yi, L., Camargo, S.J., Hu, Y., Liu, K., Chen, H., Liao, Q., Shi, J., 2017. Impact of ocean warming on tropical cyclone track over the western North Pacific: a numerical investigation based on two case studies. *J. Geophys. Res. Atmos.* 122, 8617–8630.
- Tan, H., Cai, R., 2018. What caused the record-breaking warming in East China Seas during August 2016? *Atmos. Sci. Lett.* 19, e853.
- Wheeler, M.C., Hendon, H.H., 2004. An all-season real-time multivariate MJO index: Development of an index for monitoring and prediction. *Mon. Weather Rev.* 132, 1917–1932.
- Yao, Y.L., Wang, C.Z., 2021. Variations in Summer Marine Heatwaves in the South China Sea. *J. Geophys. Res. Oceans* 126 (10), e2021JC017792.
- Yuan, Y., Yang, H., Li, C.Y., 2014. Possible influences of the tropical Indian Ocean Dipole of the eastward propagation of MJO. *J. Trop. Meteorol.* 20 (2), 173–180.
- Yuan, Y., Gao, H., Liu, Y.J., 2017. Analysis of the characteristics and causes of precipitation anomalies over Eastern China in the summer of 2016. *Meteorol. Monogr.* 43, 115–121 (in Chinese).
- Zhao, S., Jin, F.-F., Stuecker, M.F., 2019. Improved predictability of the Indian Ocean Dipole using seasonally modulated ENSO forcing forecasts. *Geophys. Res. Lett.* 46 (16), 9980–9990.